

Testing statistical isotropy in Cosmic Microwave Background Polarization maps

Pranati K. Rath^{1,2*}, Pramoda Kr. Samal^{3†}, Srikanta Panda³, Debesh D. Mishra⁴

July 23, 2022

¹ Institute of High energy Physics, Chinese Academy of Sciences, Beijing 10049, China

²Theoretical Physics Center for Science Facilities, Chinese Academy of Sciences, Beijing 100049, China

³ Dept. of Physics, Utkal University, Bhubaneswar, Odisha, 751004, India

⁴ Wuhan University Of Technology, Wuhan, China

Abstract

We apply our symmetry based Power tensor technique to test possible signal of anisotropy in PLANCK Polarization maps. On a wide range of angular scales ($l = 40 - 150$), our preliminary analysis detect statistically significant signal of anisotropy in all foreground cleaned PLANCK maps. We also study the effect of residual foreground present in the galactic plane using both common UPA77 polarization mask and individual polarization mask of COMMANDER, NILC, SMICA and SEVEM provided by PLANCK team.

1 Introduction

The standard cosmological model is based on the postulate that the universe is homogeneous and isotropic on large distance scales. However there exist many observations which suggest that this postulate is violated. The first indication of anisotropy came from the analysis of radio polarization from distant radio galaxies [1, 2, 3]. The authors found that the polarization offsets, after eliminating the effect of Faraday rotation show a dipole pattern on the sky and the dipole axis points towards the Virgo cluster of galaxies, very close to the direction of the CMB dipole [2]. The optical polarization from distant quasars show alignment over very large distance scales [4, 5]. The distance scale of alignment is found to be of order 1 Gpc [3]. One can define a preferred axis by considering the two points of each source. The axis points in the direction where the correlation maximize and is again close to the CMB dipole axis. The CMB quadrupole and octopole also indicates a preferred direction pointing towards the virgo cluster [6, 7, 8, 9, 10, 36, 11]. This phenomenon is known as the virgo alignment. Besides the virgo alignment there also exist statistically

*email:pranati@ihep.ac.cn

†email:pkksamal@iopb.res.in

significant signal of the hemispherical power asymmetry [12, 13, 14, 15, 16, 17, 18, 19, 20], parity asymmetry [21, 22, 23, 24, 25, 26] and a region of significant temperature decrement known as cold spot [27, 28, 29, 30, 31].

A large number of papers have been studied the CMB anisotropies in great detail [32, 56, 60, 6, 9, 44, 8, 45, 67, 68, 59]. General methods have been developed in order to test the signal of statistical isotropy in the CMB data [64, 65, 66, 6, 44, 36, 49]. In Refs. [36, 49], the authors proposed a symmetry based method for testing the isotropy of CMB temperature data known as “Power tensor”. The method is based on identifying invariant relation between different multipoles. For each multipole $l \geq 2$, there are three rotationally invariant eigenvalues of the power tensor, A_{ij} , defined by

$$A_{ij} = \frac{1}{l(l+1)} \sum_{m,m'} a_{lm}^* (J_i J_j)_{mm'} a_{lm'} . \quad (1)$$

Here J_i ($i = 1, 2, 3$) are the angular momentum operators in the representation l . The sum of the three eigenvalues reproduce the usual angular power spectrum C_l . The remaining independent combinations of eigenvalues provide information about the isotropy of the sample. Statistical anisotropies in the CMB data lead to statistical fluctuations in the eigenvalues and these fluctuations are measured by power entropy [36, 49, 52].

In this paper we perform an analysis to anticipate the possible anisotropy signal (if any) in the PLANCK CMB polarization data using our symmetry based method [36, 49, 52] and its relation to the existing anomalies in the CMB temperature data. The violation of statistical isotropy can arise from some physical effect, such as contamination due to foregrounds or correlation of noise. Here in this paper we do not make any attempt to find the exact cause of anisotropy.

The paper is organized as follows. In section 2, we review the theory of CMB polarization. Then we define our statistics in section 3 to analyze the data. We give all the information about the data used in our analysis in section 4 and discuss the result in section 5. In section 5, we first give the result for the PLANCK data without masking the galactic region and then give the result by masking the galactic region. Finally we summarize our work in section 6.

2 CMB Polarization Maps

The full sky CMB signal is described by the stokes parameters I , Q , U and V . The stokes parameter I , represents the temperature field and linear combination of the stokes parameters (Q, U) , represent the polarization field. The CMB temperature fluctuation is a scalar random field and conventionally it can be expanded in terms of the spherical harmonics as

$$T(\hat{n}) = \sum_{lm} a_{lm} Y_{lm}(\hat{n}). \quad (2)$$

The CMB polarization is caused by the Thomson Scattering at the last scattering surface. The WMAP and PLANCK team provides the basic maps of the polarization in terms of the stokes parameters Q and U . The stokes parameter V , which describe the circular polarization is ignored as it can not be generated through Thomson scattering. Instead of the stokes parameters Q and U , it is useful to employ the special combination of these parameters as $Q + iU$ and $Q - iU$, which transform as spin-2 fields under rotation of the coordinates by an angle ϕ . From now onwards

we use the notation of Ref. [53] for the polarization fields. Under a rotation by an angle ϕ , the combination of Q and U behave as spin ± 2 fields on a sphere, viz.

$$(Q \pm iU)'(\hat{n}) = e^{\mp 2i\phi} (Q \pm iU)(\hat{n}), \quad (3)$$

In analogy to the expansion of temperature field in terms of the spherical harmonics, $Y_{lm}(\hat{n})$, there also exist a set of spin- s spherical harmonics ${}_s Y_{lm}(\hat{n})$, in terms of which one can expand the spin- s functions. We may, therefore, expand $(Q \pm iU)(\hat{n})$ in terms of the spin-2 spherical harmonics $\pm 2 Y_{lm}(\hat{n})$ as

$$(Q \pm iU)(\hat{n}) = \sum_{lm} a_{\pm 2,lm} \pm 2 Y_{lm}(\hat{n}). \quad (4)$$

For Q and U to be real, the expansion coefficients must satisfy, $a_{-2,lm}^* = a_{2,l-m}$. Using the following identities for the spin raising and lowering operators \mathfrak{D} and $\bar{\mathfrak{D}}$, spin-0 objects can be constructed from spin-2 Q and U fields as

$$\mathfrak{D} {}_s Y_{lm} = \sqrt{[(l-s)(l+s+1)]} {}_{s+1} Y_{lm} \quad (5)$$

$$\bar{\mathfrak{D}} {}_s Y_{lm} = -\sqrt{[(l+s)(l-s+1)]} {}_{s-1} Y_{lm}. \quad (6)$$

Hence, we get

$$\bar{\mathfrak{D}}^2 (Q + iU)(\hat{n}) = \sum_{lm} \sqrt{\frac{(l+2)!}{(l-2)!}} a_{2,lm} Y_{lm}(\hat{n}) \quad (7)$$

$$\bar{\mathfrak{D}}^2 (Q - iU)(\hat{n}) = \sum_{lm} \sqrt{\frac{(l+2)!}{(l-2)!}} a_{-2,lm} Y_{lm}(\hat{n}). \quad (8)$$

Finally the standard E and B mode polarization field which are invariant under rotation can be expressed as

$$\begin{aligned} E(\hat{n}) &= -\frac{1}{2} [\bar{\mathfrak{D}}^2 (Q + iU) + \bar{\mathfrak{D}}^2 (Q - iU)] \\ &= \sum_{lm} \sqrt{\frac{(l+2)!}{(l-2)!}} a_{lm}^E Y_{lm}(\hat{n}) \end{aligned} \quad (9)$$

$$\begin{aligned} B(\hat{n}) &= \frac{i}{2} [\bar{\mathfrak{D}}^2 (Q + iU) - \bar{\mathfrak{D}}^2 (Q - iU)] \\ &= \sum_{lm} \sqrt{\frac{(l+2)!}{(l-2)!}} a_{lm}^B Y_{lm}(\hat{n}) \end{aligned} \quad (10)$$

where a_{lm}^E and a_{lm}^B are the spherical harmonic coefficients of E -mode and B -mode polarization fields. These spherical harmonic coefficients are defined as linear combinations of $a_{\pm 2,lm}$ as

$$\tilde{a}_{lm}^E = -\frac{1}{2} (\tilde{a}_{2,lm} + \tilde{a}_{-2,lm}) \quad (11)$$

$$\tilde{a}_{lm}^B = \frac{i}{2} (\tilde{a}_{2,lm} - \tilde{a}_{-2,lm}) \quad (12)$$

Here we restrict our attention to the harmonic coefficients of $E(\hat{n})$ -mode, i.e a_{lm}^E , to study the statistical isotropy of PLANCK polarization maps.

3 Statistics

The angular orientation of each mode is probed by a unique orthonormal frame $e_k^\alpha(l)$ and rotationally invariant eigenvalues $\Lambda_\alpha(l)$ of the power tensor A , defined in the Eq. (1). In terms of these, the power tensor matrix A for each multipole l may be expressed as

$$A_{ij} = \sum_\alpha e_i^\alpha (\Lambda^\alpha)^2 e_j^{\alpha*}. \quad (13)$$

We do not explicitly display the index l when it is obvious. The dispersion of eigenvalues for each multipole l is parametrized by the power entropy defined by

$$S_p = - \sum_\alpha (\tilde{\lambda}^\alpha) \log(\tilde{\lambda}^\alpha) \quad (14)$$

where $\tilde{\lambda}^\alpha = \frac{\lambda^\alpha}{\sum_\alpha \lambda^\alpha}$. An ideal case of isotropy, where all the three eigenvalues are degenerate and equal to $\sqrt{\frac{C_l}{3}}$, gives the maximum power entropy, $S_p \rightarrow \log(3)$ and the case of “pure state”, where one of the eigenvalue is the total power and other two vanishes, gives the zero power entropy $S_p \rightarrow 0$. So for our observational data the range of power entropy is $0 \leq S_p \leq \log(3)$. Hence the low power entropy compared to that of isotropy is the measure of anisotropy in the data.

We call the eigenvector, $e_k^\alpha(l)$, corresponding to the maximum eigenvalue of the power tensor defined in Eq. (1) as the “principal axis”. The dispersion of principal eigenvector across different multipoles l is parametrized in terms of the alignment entropy, defined by

$$S_X = -\text{tr}(\rho_X \log(\rho_X)) \quad (15)$$

where $\rho_X = \frac{X}{\text{tr}X}$ is the normalization of the 3×3 matrix X_{ij} defined by

$$X_{ij} = \sum_{l_{min}}^{l_{max}} e^i(l) e^j(l). \quad (16)$$

The power entropy and the alignment entropy are independent of each other. The very unusual low value of S_X compared to $\log(3)$ confirms the violation of isotropy.

The significance of anisotropy is determined by comparing the data statistic value with that of simulations and the significance is quoted by the P -value. The P -value is defined as the probability that a random realization may yield a statistic larger than that seen in data. The signature level of collection of P -values is estimated using the binomial distribution of “pass” and “fail” outcomes. The probability to encounter k instances of passing defined by probability P in n trials is

$$P_{min}(k, P, n) = \frac{P^k (1-P)^{n-k} n!}{(n-k)! k!} \quad (17)$$

In assessing many P -values, we report the cumulative binomial probabilities as

$$P_{bin}(k \geq k_*, P, n) = \sum_{k=k_*}^n P_{bin}(k, P, n) \quad (18)$$

4 Data Used

For our study we use the four foreground cleaned polarization maps named as COMMANDER RULER, NILC, SEVEM and SMICA provided by PLANCK team [33, 20]. These maps are generated by linearly combining the CMB raw maps which are available at nine widely separated frequencies from 30 to 857 GHz. These maps differ from one another depending on the component separation algorithm used in the clean map making procedure. Due to high level of noise present in the polarization maps and also due to the presence of residual foregrounds even after cleaning, any signature of large scale anisotropy has to be interpreted with care. The cleaned polarization maps are provided at a resolution of $10'$ FWHM with $N_{side} = 1024$. These maps are not reliable at low- l upto $l = 40$ [33, 20], hence we put the lower cut on the multipole as $l = 40$. As noise contribute dominantly for the polarization map, one can not do the analysis for higher multipole without taking into account the noise. Hence we restrict our analysis upto $l = 150$. To start our analysis, we first extract the E -mode polarization map from Q and U map and then downgrade the E -mode CMB map and the mask maps which are at higher resolution with $N_{side} = 1024$ to the lower resolution with $N_{side} = 512$. We first do the analysis for all the four foreground cleaned PLANCK E -mode polarization maps without removing the residual foregrounds present in the galactic region. Then we mask the galactic region with the polarization mask and construct the “fullsky” E -mode polarization maps and repeat our analysis.

The fullsky maps are constructed following the procedure as given in Refs.[54, 18, 50, 19]. We extract the spin-0 E -mode field from the spin-2 stokes parameters Q and U using the Eq. (11). We then apply the polarization mask on the E -mode polarization map to remove the residual contamination still present in the galactic region even after cleaning. We fill the masked region with the simulated map obtained using the master algorithm [54] to get fullsky E -mode data polarization map. Here we will briefly review the master algorithm [54].

The pseudo angular power spectrum of the masked sky, \tilde{C}_l^E , can be defined as

$$\tilde{C}_l^E = \frac{1}{2l+1} \sum_{m=-l}^l a_{lm}^E a_{lm}^{*E}. \quad (19)$$

Now the full sky angular power spectrum C_l^E , can be obtained as

$$\langle \tilde{C}_l^E \rangle = \sum_{l'} M_{ll'} C_{l'}^E \quad (20)$$

where $M_{ll'}$ describes the mode-mode coupling matrix. We compute $M_{ll'}$ from the polarization mask used for our analysis. We then take this full sky C_l^E to generate the fullsky E -mode simulated polarization map using Healpix [55]. We then use these simulated map to fill the masked region and get fullsky E -mode data polarization map. In this way we generate 100 foreground cleaned fullsky E -mode data polarization maps and compute their statistics. The data value is the average of these 100 fullsky maps.

For the masking purpose we use both common polarization mask, *UPA77* and the polarization masks provided with each cleaned PLANCK polarization maps. These maps are shown in the Fig. (1) and (2). The common polarization mask, *UPA77* covers 78% of the sky fraction whereas, the other polarization masks named as COMMANDER, NILC, SMICA and SEVEM covers 83%, 96%, 85% and 79% of the sky fraction respectively. The significance of anisotropy

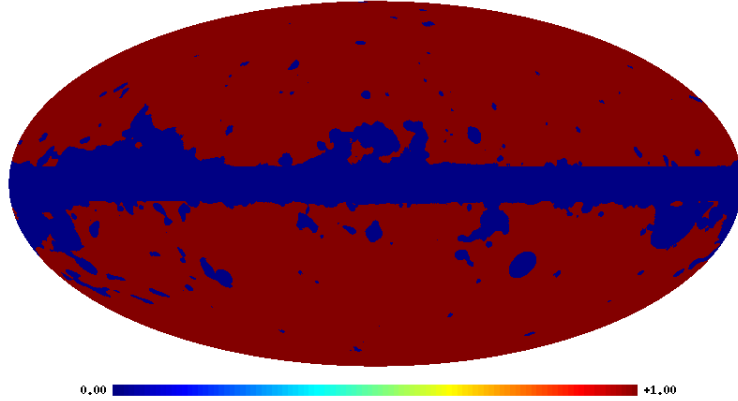


Figure 1: The common *UPA77* polarization mask at $Nside = 1024$

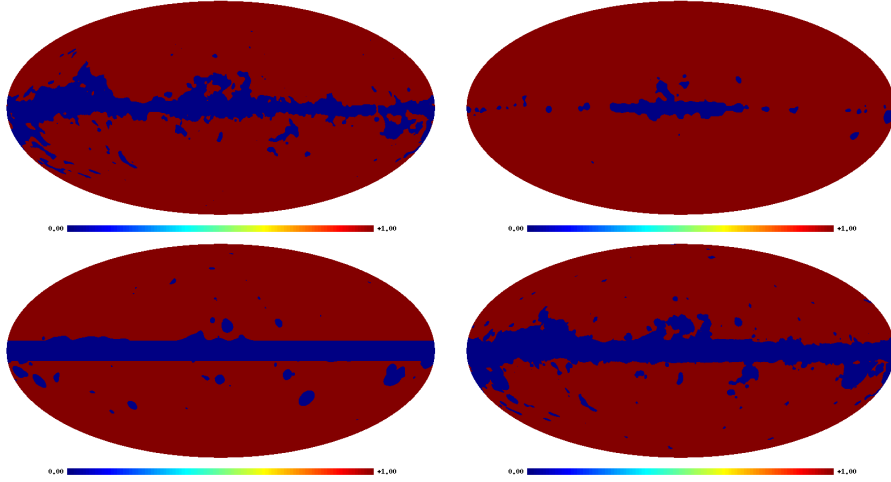


Figure 2: The polarization mask of COMMANDER, NILC, SEVEM and SMICA respectively at $Nside = 1024$. The top row represents the polarization mask of COMMANDER and NILC map and the bottom row represents for SEVEM and SMICA.

is obtained by comparing the data statistic value with 4000 random realizations. For our analysis we neglect the noise contribution as we do not know how to implement them now. The random realizations are obtained from the best fit theoretical angular power spectrum(C_l^{th}). The best fit C_l^{th} are generated using PLANCK cosmological parameters [35, 34] as the input to CAMB software [62, 63]. The values of the PLANCK cosmological parameters are baryon matter density $\Omega_b h^2 = 0.0222$, cold dark matter density $\Omega_c h^2 = 0.1203$, neutrino energy density $\Omega_\nu h^2 = 0.00064$, density parameter for cosmological constant $\Omega_\Lambda = 0.6823$, Hubble parameter H_0 with $h = 0.6712$, spectral index of the primordial power spectrum $n_s = 0.96$, and amplitude of the primordial power spectrum $A_s = 2.09 \times 10^{-9}$ with the reionization optical depth $\tau = 0.078$ [35, 34]. Then we use this best fit C_l^{th} to generate the random realizations of the CMB map using HEALPIX software [55].

<i>Map</i>	<i>Multipoles</i>
<i>COMMANDER</i>	40, 41, 42, 45, 51, 52, 57, 60, 65, 66, 76, 92, 95, 116, 122, 135, 146, 147
<i>NILC</i>	40, 44, 45, 46, 49, 51, 54, 56, 59, 60, 72, 74, 76, 79, 81, 83, 89, 90, 92, 93, 95, 98, 100, 102, 104, 108, 116, 118, 119, 120, 122, 123, 125, 128, 129, 131, 133, 135, 142, 143, 146, 147, 148
<i>SEVEM</i>	40, 41, 44, 45, 49, 51, 52, 53, 55, 60, 62, 66, 72, 76, 80, 84, 85, 92, 93, 94, 102, 104, 105, 108, 116, 123, 131, 135, 137, 139, 141, 146, 147, 148, 149
<i>SMICA</i>	40, 45, 51, 54, 56, 60, 62, 76, 81, 83, 92, 94, 95, 98, 102, 104, 108, 116, 123, 131, 139, 148

Table 1: List of multipoles with $P \leq 0.05$ for power entropy for PLANCK cleaned E -mode polarization maps without masking the galactic region.

5 Power entropy and its statistical Significance

5.1 Without masking the galactic region

We first take the PLANCK polarization map without masking the galactic region, extarct the E -mode polarization map and then downgrade the map to the lower resolution with $N_{side} = 512$. We compute the power entropy, S_p , from the E -mode polarization map for each multipole in the chosen multipole range $l = 40 - 150$. The statistical significance of the power entropy for the polarization map is studied using 4000 isotropic random CMB E -mode polarization maps. Fig. (3) shows the null distribution of power entropy for the multipole range $l = 40 - 150$. Fig. (4) shows P -value of the COMMANDER, NILC, SEVEM and SMICA maps. We define the P -value as the relative frequency of occurrence of $P = 0.05$ or less as compared to that of simulation results in the chosen multipole range. The horizontal dashed line indicates $P = 0.05$. Multipoles which are below the dashed line indicate the violation of isotropy for that particular multipole. The list of these multipoles are listed in the Table (1). From the Table (1), we find that there are 18, 43, 35 and 22 number of multipoles which have $P \leq 0.05$ for COMMANDER, NILC, SEVEM and SMICA E -mode polarization maps respectively. The threshold values (upper bounds of P - values) for these power entropies estimated for COMMANDER, NILC, SEVEM and SMICA maps are given by $P = 0.045, 0.049, 0.049$ and 0.038 respectively. Using Eq. (18), we compute the cumulative probability to estimate the significance of anisotropy. The total number of independent trials for the range $40 \leq l \leq 150$ is 111. From the binomial distribution the *cumulative* probabilities of obtaining $P_{bin}(k \geq k_{data}, P_{data}, 111)$ are shown in Table (2) for PLANCK polarization data. From the Table (2), we can see that the cumulative probability for NILC and SEVEM E -mode polarization map is very very small compared to COMMANDER and SMICA. The entropy distribution leading these P -values with a contour of 95% confidence level is shown in Fig. (5). The entropy value of the multipoles which are below 5% are shown by red points below the countour. The violation of statistical isotropy is clearly found in all the PLANCK cleaned polarization maps. One can easily conclude that these anomalies are may be due to the presence of residual foregrounds in the galactic region of the cleaned map. Next we try to ignore the heavily contaminated galactic region to study for our statistical isotropy following the filling procedure described in the section 4.

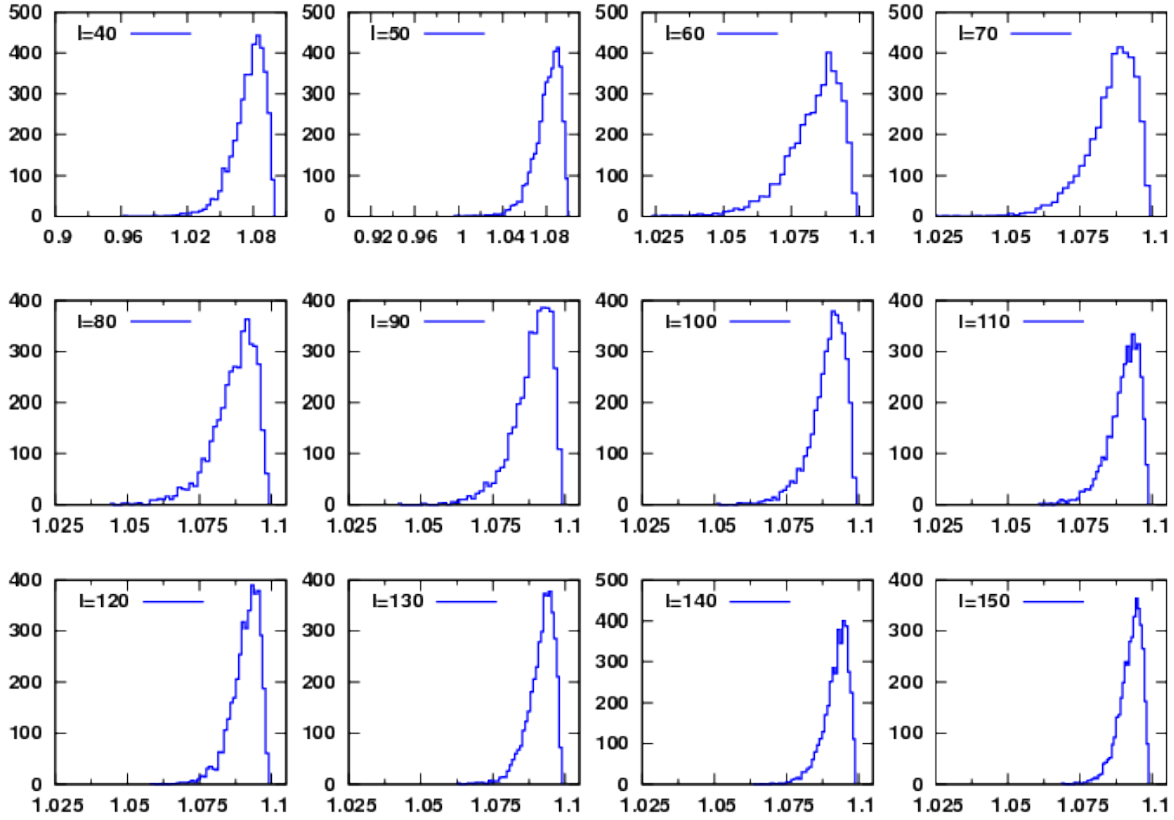


Figure 3: Histogram of the power entropy S_P obtained from 4000 E -field simulated maps for the multipole range $40 \leq l \leq 150$ at intervals of 10 multipole.

5.2 With masking the galactic region

In this section, we present the result obtained from the constructed fullsky E -mode data polarization map [18, 19] discussed in section 4. For this we fill the masked regions with the maps obtained from the master algorithm following the Ref.[54]. We first use the common *UPA77* mask to all the four cleaned *PLANCK* E -mode polarization maps and then estimate the statistic value. Then we use the *COMMANDER* polarization mask on *COMMANDER*, *NILC* polarization mask on *NILC*, *SMICA* polarization mask on *SMICA* and *SEVEM* polarization masks on *SEVEM* E -mode polarization map and estimate their statistic value. Fig. (6) shows P -values of the *COMMANDER*, *NILC*, *SEVEM* and *SMICA* maps having value 0.05 or less as compared to that of simulations in the chosen multipole range using *UPA77* polarization mask. Multipoles which are below the horizontal dashed line referring $P = 0.05$ indicate the violation of isotropy for that particular multipole.

Map	<i>COMMANDER</i>	<i>NILC</i>	<i>SEVEM</i>	<i>SMICA</i>
Significance	0.24×10^{-5}	0.36×10^{-26}	0.51×10^{-18}	0.20×10^{-9}

Table 2: Net significance of observing cumulative probability for *PLANCK* cleaned E -mode polarization maps without masking the galactic region

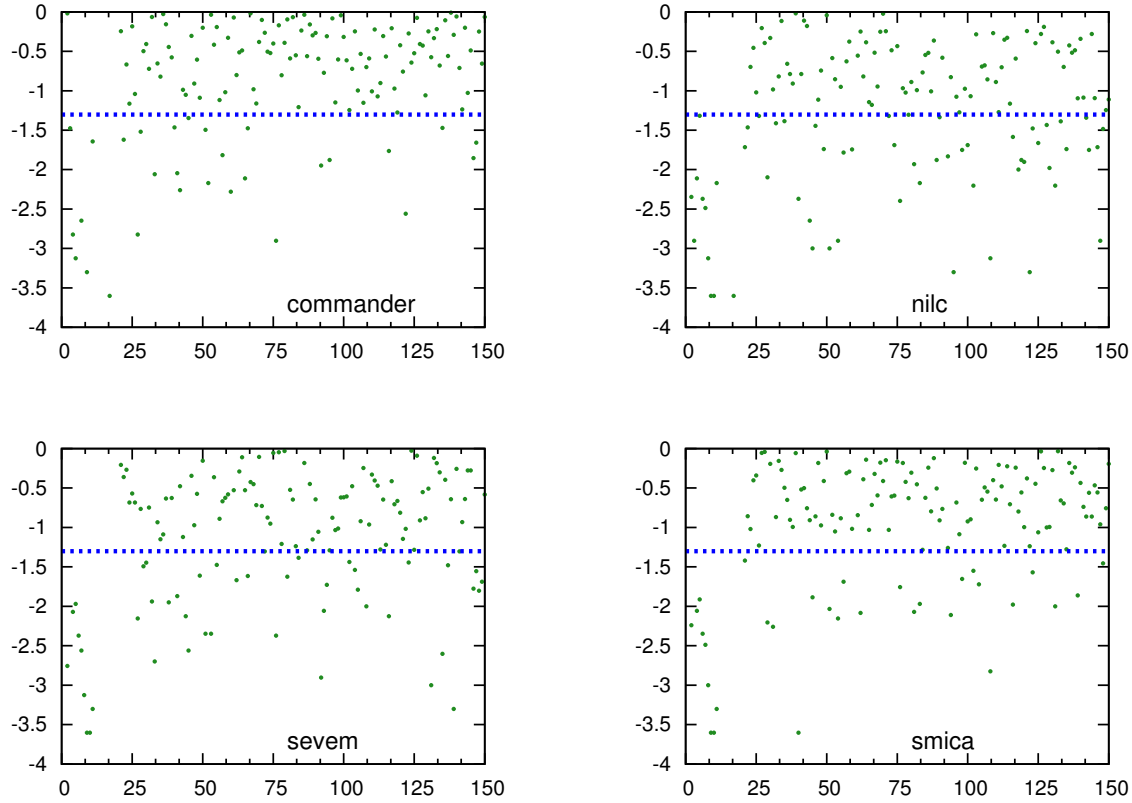


Figure 4: $\log_{10}(P)$ —values of the power entropy for the range $40 \leq l \leq 150$ for COMMANDER, SMICA, NILC and SEVEM E -mode polarization maps without masking the galactic region. The dashed horizontal line shows $P = 0.05$.

By filling the masked region using common *UPA77* mask, we see that there are only 11, 18, 13 and 14 multipoles having $P \leq 0.05$ compared to that of simulations for COMMANDER, NILC, SEVEM and SMICA E -mode polarization maps respectively. Similarly by filling the masked region with the individual masks as explained above, we see that there are 13, 27, 17 and 18 multipoles with $P \leq 0.05$ for COMMANDER, NILC, SEVEM and SMICA E -mode polarization maps respectively. The list of the multipoles having $P \leq 0.05$ for both the cases are given in the Table (3) and Table (5) and the corresponding cumulative probabilities are given in the Table (4) and Table (6). From the Table (4) and Table (6), we can see that the cumulative probability value is larger than PLANCK cleaned maps without masking the galactic region, hence the significance value decreases as we use the fullsky map obtained by masking the galactic region. The entropy distribution for the fullsky map leading these P -values with a countour of 95% confidence level is shown in Fig. (7). The red points show the entropy value of the multipoles which are below 5%. This contour plot clearly show the multipoles which are potentially inconsistent with the isotropic prediction. Here we only give the contour plot for the fullsky map using common *UPA77* polarization mask. Since the *NILC* polarization mask covers 96% of the sky fraction, we get more number of multipoles which have $P \leq 0.05$ compared to fullsky map obtained using *UPA77* mask. So from here one can easily conclude that the presence of residual foreground in the cleaned map

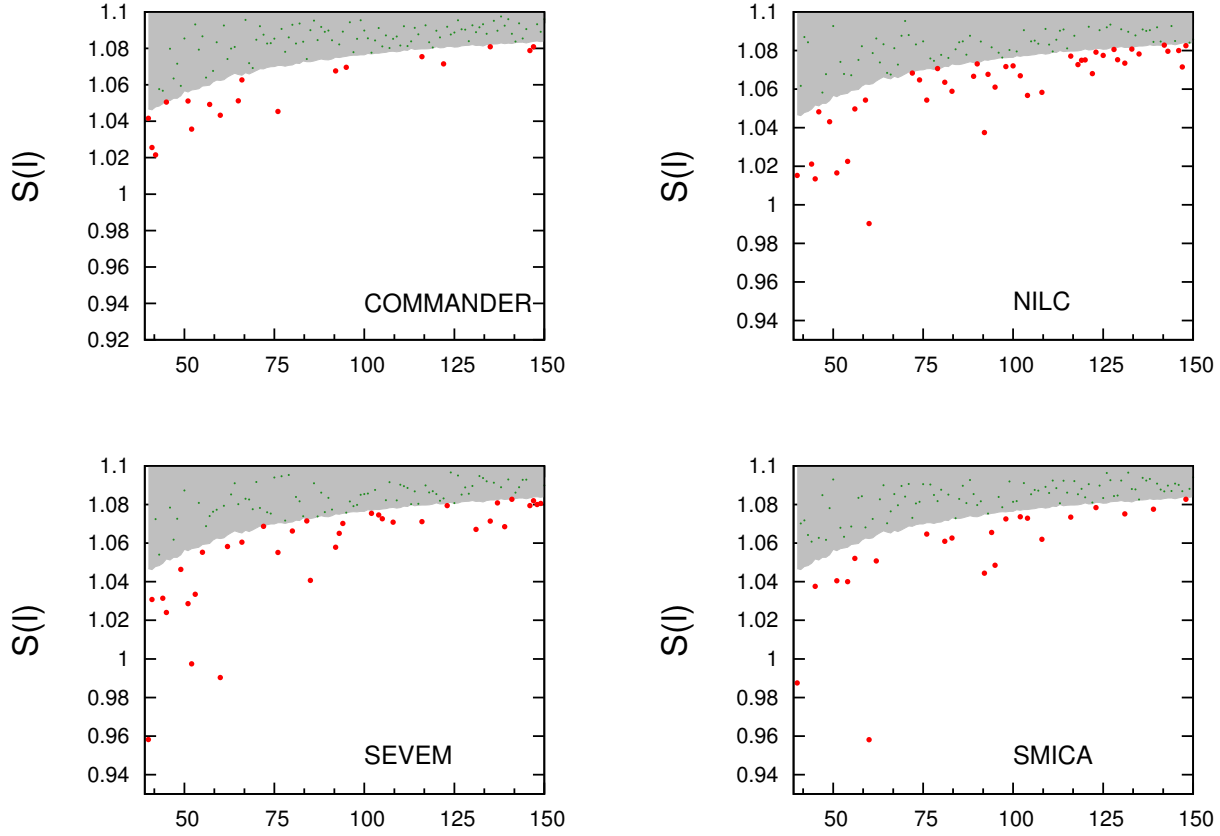


Figure 5: Distribution of the power entropy of PLANCK four fullsky E -mode polarization maps without masking the galactic region. The grey band show the 95% confidence level for the 4000 simulations and the Red dots refer to the multipoles coressponding to PLANCK data.

contributes a lot to the observed anisotropy. The anisotropy also depend on the sky fraction of the mask used to remove the galactic residual foregrounds.

<i>Map</i>	<i>Multipoles</i>
<i>COMMANDER</i>	42, 43, 49, 51, 60, 92, 108, 112, 116, 119, 122,
<i>NILC</i>	42, 45, 49, 51, 54, 56, 60, 78, 92, 93, 94, 108, 116, 118, 119, 122, 131, 142
<i>SMICA</i>	41, 42, 49, 52, 60, 73, 76, 78, 116, 118, 119, 122, 131
<i>SEVEM</i>	42, 45, 49, 51, 54, 56, 60, 78, 92, 93, 94, 108, 116, 122

Table 3: List of multipoles with $P < 0.05$ for PLANCK Fullsky cleaned E -mode polarization maps obtained by filling the map using master process [54]. Here common polarization mask *UPA77* is used to mask the galactic plane for all the maps.

<i>Map</i>	<i>COMMANDER</i>	<i>NILC</i>	<i>SEVEM</i>	<i>SMICA</i>
Significance	0.0192	0.243×10^{-5}	0.182×10^{-02}	0.811×10^{-03}

Table 4: Net significance of observing cumulative probability for Fullsky cleaned E -mode polarization maps obtained by filling the map using master process [54]. Here common polarization mask *UPA77* is used to mask the galactic plane for all the maps.

<i>Map</i>	<i>Multipoles</i>
<i>COMMANDER</i>	42, 43, 49, 51, 58, 60, 76, 92, 95, 108, 116, 119, 122,
<i>NILC</i>	40, 44, 49, 51, 54, 56, 60, 76, 83, 92, 93, 94, 95, 101, 102, 104, 108, 116, 118, 119, 120, 122, 125, 131, 135, 147, 149
<i>SMICA</i>	41, 42, 45, 49, 51, 52, 58, 60, 76, 78, 106, 116, 118, 119, 122, 131, 139
<i>SEVEM</i>	40, 42, 45, 49, 51, 52, 54, 60, 78, 84, 92, 93, 94, 108, 116, 122, 129, 131

Table 5: List of multipoles with $P < 0.05$ for power entropy for PLANCK Full sky cleaned E mode polarization maps obtained by filling the map obtained using master process with different mask [54]. Here polarization mask provided with each cleaned map is used to mask the galactic plane for all the maps.

<i>Map</i>	<i>COMMANDER</i>	<i>NILC</i>	<i>SEVEM</i>	<i>SMICA</i>
Significance	0.3142×10^{-02}	0.8564×10^{-12}	0.261×10^{-04}	0.331×10^{-06}

Table 6: Net significance of observing cumulative probability fro Full sky cleaned E -mode polarization maps obtained by filling the map obtained using master process with different mask [54]. Here polarization masks provided with each cleaned maps are used to mask the galactic palne for all the maps.

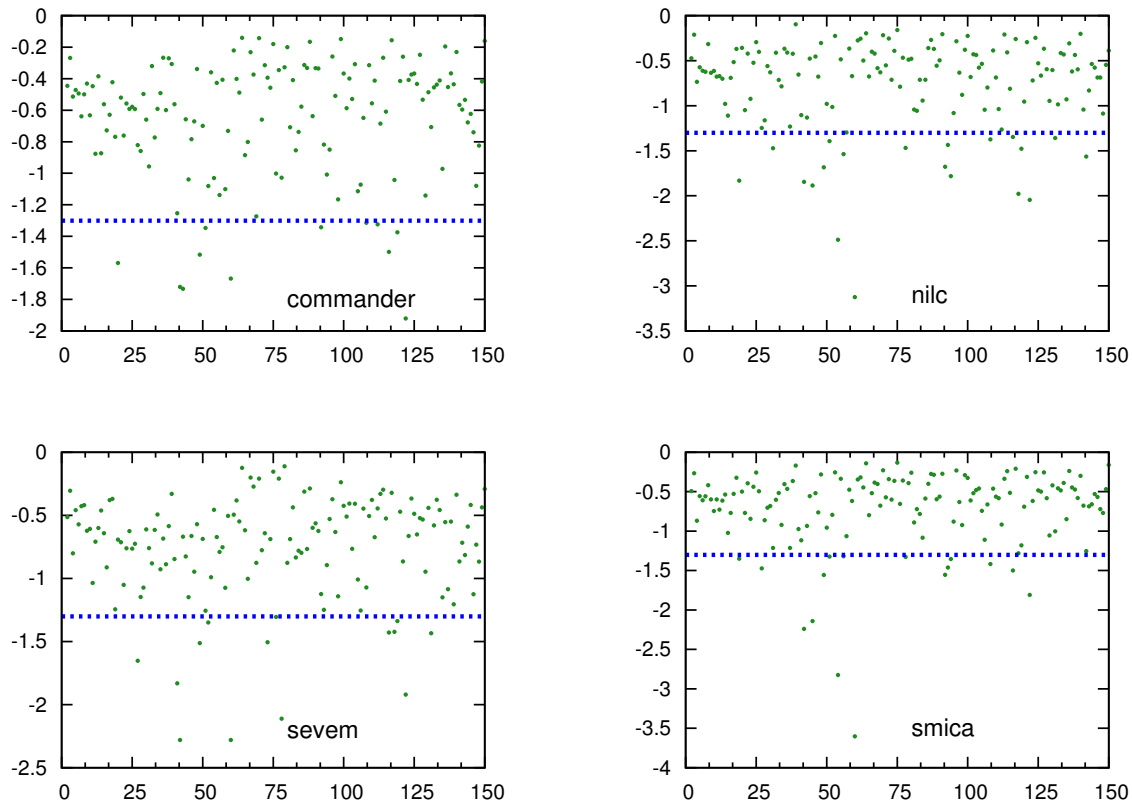


Figure 6: $\log_{10}(P)$ –values of the power entropy for the range $40 \leq l \leq 150$ for COMMANDER, SMICA, NILC and SEVEM polarization maps after filling the galactic region with the common UPA77 polarization mask. The dashed horizontal line shows $P = 0.05$.

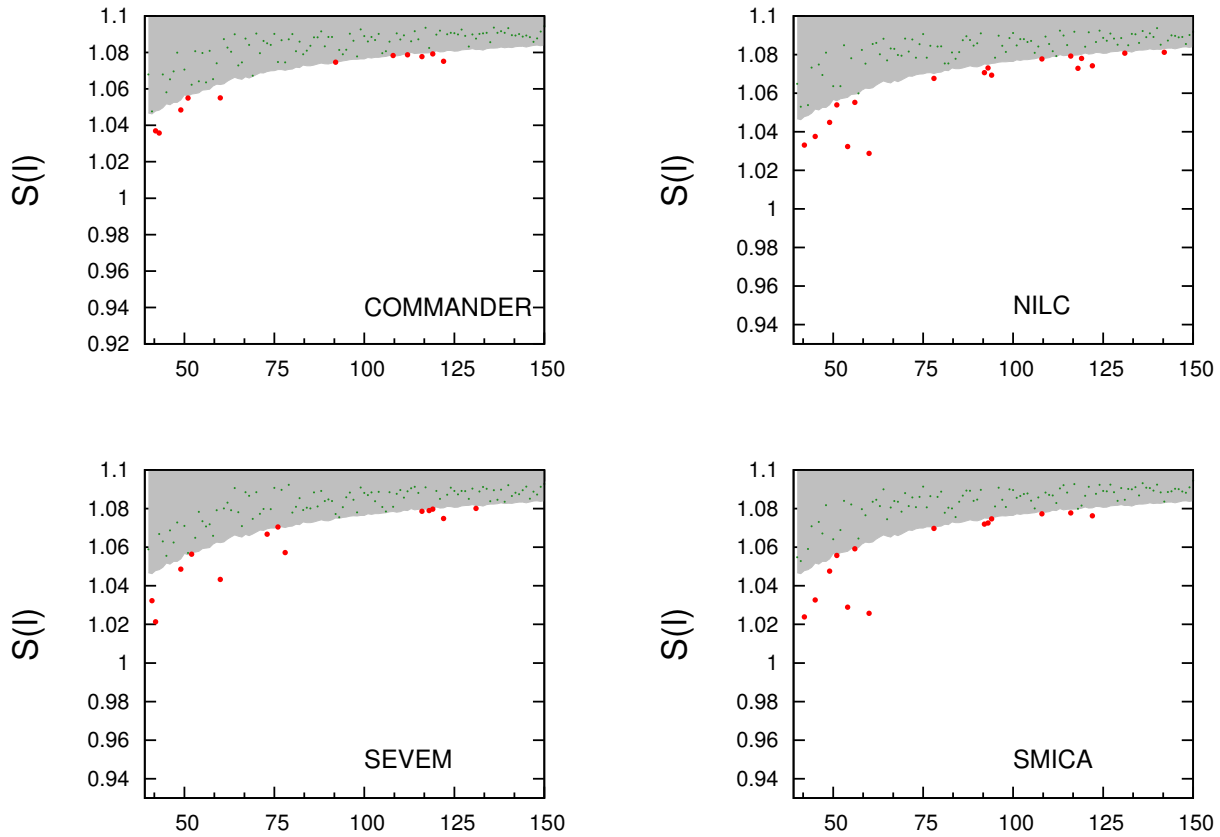


Figure 7: Distribution of the power entropy of PLANCK four fullsky E -mode polarization maps. The grey band show the 95% confidence level for the 4000 simulations and the Red dots refer to the multipoles coressponding to PLANCK data. Here we use UPA77 polarization mask to mask the galactic region.

6 Conclusion

We have used all the foreground cleaned PLANCK Q and U polarization maps and extracted the E -mode polarization maps from them. We have applied our symmetry based power tensor method to test for statistical anisotropy in these maps. For our preliminary analysis we have chosen the multipole range as $l = 40 - 150$ and neglected the contribution of noise in this range. We have computed the power entropy measuring the dispersion of the eigenvalues for each multipole from the data and compare it with 4000 simulations to estimate its significance. We found very strong signal of violation of statistical isotropy in all foreground cleaned sky maps. As these maps contain significant signal of residual contamination in the galactic plane and it is reasonable to attribute the signal to this foreground residual. We have also studied the maps after masking out the galactic plane in order to remove the residual foreground. In this case the strong signal of anisotropy was removed to some extent but we still found signal of anisotropies inconsistent with Statistical isotropy. This may be due to detector noise or due to the fundamental cosmological origin. In this work we don't make any attempt to find the exact cause of anisotropy.

Acknowledgements

The results in this paper have been derived using publicly available HEALPIX package [55]. We acknowledge the use of PLANCK data available from NASA's LAMBDA site (<http://lambda.gsfc.nasa.gov/>).

References

- [1] P. Birch, *Nature* **298**, 451 (1982).
- [2] P. Jain and J.P. Ralston, *Modern Physics Letters A* **14**, 417 (1999).
- [3] P. Jain, G. Narain, and S. Sarala, *Mon. Not. R. Astron. Soc.* **347**, 394 (2004).
- [4] D. Huterer, *Astron. Astrophys.* **332**, 410 (1998).
- [5] D. Huterer and H. Lamy, *Astron. Astrophys.* **367**, 381 (2001).
- [6] C. J. Copi, D. Huterer, and G. D. Starkman, *Phys. Rev. D* **70**, 043515 (2004).
- [7] J.P. Ralston and P. Jain, *International Journal of Modern Physics D* **13**, 1857 (2004).
- [8] A. de Oliveira-Costa, M. Tegmark, M. Zaldarriaga, and A. Hamilton, *Phys. Rev. D* **69**, 063516 (2004).
- [9] D. J. Schwarz, G. D. Starkman, D. Huterer, and C. J. Copi, *Physical Review Letters* **93**, 221301 (2004).
- [10] L. R. Abramo, L. Sodré, Jr., and C. A. Wuensche, *Phys. Rev. D* **74**, 083515 (2006).
- [11] L. R. Abramo *et al.*, *Phys. Rev. D* **74**, 063506 (2006).

- [12] H. K. Eriksen *et al.*, *Astrophys. J.* **605**, 14 (2004).
- [13] H. K. Eriksen, P.B. Lilje, A. J. Banday, and K.M. Górska, *Astrophys. J. Supp.* **151**, 1 (2004).
- [14] H. K. Eriksen *et al.*, *Astrophys. J.* **612**, 64 (2004).
- [15] F.K. Hansen, A.J. Banday, K.M. Gorski, H.K. Eriksen, and P.B. Lilje, *Astrophysical Journal* **704**, 1448 (2009).
- [16] D. Hanson, and A. Lewis, *Phys. Rev. D* **80**, 063004 (2009).
- [17] J. Hoftuft, H. K. Eriksen, A. J. Banday, K. M. Gorski, F. K. Hansen, and P. B. Lilje, *Astrophysical Journal* **699**, 985 (2009).
- [18] P. K. Rath, and P. Jain, *Journal of Cosmology and Astro-Particle Physics* **12**, 014 (2013).
- [19] P. K. Rath, P. K. Aluri, and P. Jain, *Phys. Rev. D* **91**, 023515 (2015).
- [20] Planck Collaboration *et al.*, *Astronomy and Astrophysics* **594**, A16 (2016).
- [21] J. Kim, and P. Naselsky, *Astrophysical Journal Letters* **714**, L265 (2010).
- [22] J. Kim, and P. Naselsky, *Phys. Rev. D* **82**, 063002 (2010).
- [23] J. Kim, and P. Naselsky, *Astrophysical Journal* **739**, 79 (2011).
- [24] P. K. Aluri, and P. Jain, *Mon. Not. R. Astron. Soc.* **419**, 3378 (2012).
- [25] P. K. Aluri, John P. Ralston, A. Weltman, ArXiv e-prints (2017)
- [26] W. Zhao, *Phys. Rev. D* **89**, 023010 (2014).
- [27] M. Cruz, E. Martinez-Gonzalez, P. Vielva, and L. Cayon, *Mon. Not. R. Astron. Soc.* **356**, 29 (2005).
- [28] M. Cruz, M. Tucci, E. Martinez-Gonzalez, and P. Vielva, *Mon. Not. R. Astron. Soc.* **369**, 57 (2006).
- [29] M. Cruz *et al.*, *Mon. Not. R. Astron. Soc.* **390**, 913 (2008).
- [30] P. Vielva, *Advances in Astronomy*, **77** (2010).
- [31] P. K. Aluri, and P. K. Rath, *Mon. Not. R. Astron. Soc.* **458**, 4269 (2016)
- [32] G. Katz, and J. Weeks, *Phys. Rev. D*, **70**, 063527 (2004)
- [33] Planck Collaboration *et al.*, *Astronomy and Astrophysics* **594**, A8 (2016).
- [34] Planck Collaboration *et al.*, *Astronomy and Astrophysics* **594**, A13 (2016).
- [35] Planck Collaboration *et al.*, *Astronomy and Astrophysics* **594**, A11 (2016).
- [36] P.K. Samal, R. Saha, P. Jain, and J.P. Ralston, *Mon. Not. R. Astron. Soc.* **385**, 1718 (2008).

- [37] P. Bielewicz *et al.*, *Astrophys. J.* **635**, 750 (2005).
- [38] P. K. Aluri, P. K. Samal, P. Jain, and J. P. Ralston, *Mon. Not. R. Astron. Soc.* **414**, 1032 (2011).
- [39] K. Land and J. Magueijo, *Physical Review Letters* **95**, 071301 (2005).
- [40] H. K. Eriksen *et al.*, *Astrophys. J.* **660**, L81 (2007).
- [41] A. Bernui, *Phys. Rev. D* **78**, 063531 (2008).
- [42] A. L. Erickcek, M. Kamionkowski, and S. M. Carroll, *Phys. Rev. D* **78**, 123520 (2008).
- [43] A. L. Erickcek, S. M. Carroll, and M. Kamionkowski, *Phys. Rev. D* **78**, 083012 (2008).
- [44] C.J. Copi, D. Huterer, D.J. Schwarz, and G.D. Starkman, *Mon. Not. R. Astron. Soc.* **367**, 79 (2006).
- [45] C. J. Copi, D. Huterer, D. J. Schwarz, and G. D. Starkman, *Phys. Rev. D* **75**, 023507 (2007).
- [46] C. L. Bennett *et al.*, *Astrophysical Journal Supplement* **192**, 17 (2011).
- [47] C. L. Bennett *et al.*, *Astrophys. J. Suppl. Series* **148**, 97 (2003).
- [48] C. L. Bennett *et al.*, *Astrophysical Journal Supplement* **208**, 20 (2013).
- [49] P. K. Samal, R. Saha, P. Jain, and J.P. Ralston, *Mon. Not. R. Astron. Soc.* **396**, 511 (2009).
- [50] P. K. Samal, R. Saha, J. Delabrouille, J., et al. *APJ* **714**, 840 (2010)
- [51] R. Kothari, P. K. Rath, and P. Jain, *ArXiv e-prints* (2015).
- [52] P. K. Rath, and P. K. Samal, *Modern Physics Letters A* **30**, 1550131 (2015).
- [53] M. Zaldarriaga, U. Seljak, *Phys. Rev. D* **55**, 1830 (1997).
- [54] E. Hivon, K. M. Górski, C. B. Netterfield, B. P. Crill, S. Prunet, and F. Hansen, *Astrophysical Journal* **567**, 2 (2002).
- [55] K. M. Gorski, E. Hivon, A. J. Banday, B. D. Wandelt, F. K. Hansen, M. Reinecke, and M. Bartelmann, *Astrophysical Journal* **622**, 759 (2005).
- [56] P. Bielewicz *et al.*, *Astrophys. J.* **635**, 750 (2005).
- [57] K. Land, and J. Magueijo, *Physical Review Letters* **95**, 071301 (2005).
- [58] L. R. Abramo, L. Sodr, Jr., and C. A. Wuensche, *Phys. Rev. D* **74**, 083515 (2006).
- [59] A. Bernui, *Phys. Rev. D* **78**, 063531 (2008).
- [60] S. Prunet, J. Uzan, F. Bernardeau, and T. Brunier, *Phys. Rev. D* **71**, 083508 (2005).
- [61] E. P. Donoghue and J. F. Donoghue, *Phys. Rev. D* **71**, 043002 (2005).

- [62] A. Lewis, A. Challinor, and A. Lasenby, *ApJ*, **538**, 473 (2000).
- [63] C. Howlett, A. Lewis, A. Hall, and A. Challinor, *J. Cosmol. Astropart. Phys.*, **04**, 027 (2012).
- [64] A. Hajian and T. Souradeep, *ArXiv Astrophysics e-prints* (2003).
- [65] A. Hajian and T. Souradeep, *Astrophys. J.* **597**, L5 (2003).
- [66] A. Hajian and T. Souradeep, *Phys. Rev. D* **74**, 123521 (2006)
- [67] K. Land and J. Magueijo, *Mon. Not. R. Astron. Soc.* **378**, 153 (2007).
- [68] E. P. Donoghue and J. F. Donoghue, *Phys. Rev. D* **71**, 043002 (2005)